Simultaneous mapping of vasculature, hypoxia and proliferation using DSC-MRI, 18F-FMISO PET, and 18F-FLT PET in relation to contrast enhancement in newly diagnosed glioblastoma

Solène Collet, Jean Sébastien Guillamo, David Hassanein Berro, Ararat Chakhoyan, Jean-Marc Constans, Emmanuèle Lechapt-Zalcman, Jean-Michel Derlon, Mathieu Hatt, Dimitris Visvikis, Stéphane Guillouet, et al.

Journal of Nuclear Medicine, published on May 20, 2021 as doi:10.2967/jnumed.120.249524

Simultaneous mapping of vasculature, hypoxia and proliferation using DSC-MRI, ^{18}F-FMISO PET, and ^{18}F-FLT PET in relation to contrast enhancement in newly diagnosed glioblastoma

Collet Solène[1,2], Guillamo Jean-Sébastien[1,3,4*], Berro David Hassanein[1,5*], Chakhoyan Ararat[1], Constans Jean-marc[1, 6], Lechapt-Zalcman Emmanuèle[1,7,8], Derlon Jean-Michel[1], Hatt Mathieu[9], Visvikis Dimitris[9], Guillouet Stéphane[10], Perrio Cécile[10], Bernaudin Myriam[1] and Valable Samuel[1]

[1] Normandie Univ, UNICAEN, CEA, CNRS, ISTCT/CERVOxy group, GIP CYCERON, Caen

[2] Radiophysics Department, Centre François Baclesse, Caen

[3] Department of Neurology, CHU de Caen

[4] Department of Neurology, CHU de Nimes

[5] Department of Neurosurgery, CHU de Caen

[6] Department of Neuroradiology, CHU de Caen

[7] Department of Pathology, CHU de Caen

[8] Department of Neuropathology, GHU Paris Psychiatry and Neuroscience, Paris

[9] LaTIM, INSERM, UMR 1101, Univ Brest, Brest

[10] Normandie Univ, UNICAEN, CEA, CNRS, ISTCT/LDM-TEP group, GIP CYCERON, Caen

Corresponding author: Dr S. Valable, ISTCT, CERVOxy group, GIP CYCERON, Bd Henri Becquerel, BP5229, 14074 CAEN, France. Phone: 33231470108; fax: 33231470222. E-mail: samuel.valable@cnrs.fr; orcid # 0000-0003-0355-0270

First author: Dr S. Collet, Department of Radiophysics, Centre François Baclesse, 3 Avenue du Général Harris, 14000 Caen. Phone: 33231470230; fax: 33231470222. E-mail: s.collet@baclesse.unicancer.fr

* equal contribution

Word count in the MS: 5403

Running title: multimodal imaging of glioblastoma

ABSTRACT

Conventional MRI plays a key role in the management of patients with high grade glioma but multiparametric MRI and PET tracers could provide further information to better characterize the tumor metabolism and heterogeneity, by identifying the regions having a high risk of recurrence. In this study, we focused on the proliferation, hypervascularization and hypoxia, all factors considered as factors of poor prognosis. They were assessed by measuring the uptake of ^{18}F-FLT, the rCBV maps and the uptake of ^{18}F-FMISO, respectively. For each modality, the volumes and high uptake sub-volumes (hotspots) were semi-automatically segmented and compared to contrast enhancement (CE) volume on T1w-Gd images, commonly used in the management of patient with glioblastoma. **Methods**: DSC MRI (31 patients), ^{18}F-FLT PET (20 patients) and/or ^{18}F-FMISO PET (20 patients), for a total of 31 patients, were performed on pre-operative glioblastoma patients. Volumes and hotspots were segmented on SUV maps for ^{18}F-FLT (using FLAB) and ^{18}F-FMISO (using mean contralateral + 3.3 SD) PET and on rCBV maps (using mean contralateral + 1.96 SD) for DSC MRI and overlaid on T1w-Gd images. For each modality, the percentage of peripheral volumes and the peripheral hotspot outside the CE volume were calculated. **Results:** All tumors showed high proliferation, hypervascularization and hypoxic regions. Images also showed pronounced heterogeneity of both tracers uptake and rCBV maps, within each individual case. Overlaid volumes on T1w-Gd images showed that some proliferative, hypervascularization and hypoxic regions extended beyond the CE volume but with marked differences between patients. The ranges of peripheral volume outside the CE volume were [1.6% - 155.5 %], [1.5% – 89.5%] and [3.1% - 78.0%] for ^{18}F-FLT, rCBV and ^{18}F-FMISO respectively. All patients had hyperproliferative hotspots outside CE volume, whereas hotspots of hypervasculature and hypoxia were mainly

detected within the enhancing region. **Conclusion**: The spatial analysis of the multiparametric maps with the segmented volumes and hotspots provides valuable information to optimize the management and treatment of the patients with glioblastoma.

Key words: Proliferation, vasculature, hypoxia, MRI, PET, glioblastoma.

INTRODUCTION

Despite the use of aggressive treatments (*1*), glioblastoma remains one of the deadliest human cancers characterized by a 5 years survival of 6.8% (*2*). Glioblastoma are highly heterogeneous tumors characterized by a strong interpatient heterogeneity illustrated at both, the molecular (*3*,*4*) and the macroscopic levels. More importantly, glioblastoma are also characterized by a pronounced intratumoral heterogeneity (*5*) which is macroscopically visible on conventional MRI with regions of necrosis and contrast enhancement (*6*), and has been associated to a large range of response to therapies (*7*).

Among the various pathophysiological parameters that may influence patient survival, two keys parameters (proliferation and invasion) were considered to be predictive of patient survival (*8*). Interestingly, the dynamic interactions between tumor cells, vasculature and hypoxia is also considered as a key feature that s tumor growth (*9*–*11*).

While various works have been performed to address the spatial relationship between pairs of parameters (*10*,*12*–*17*), the concomitant and quantitative measurement of these three parameters remains challenging and has been performed only on histology (*9*) which lacks the overall overview of the entire 3D tumor volume.

Until now, conventional MRI with the so-called contrast enhancement (CE) area remains the most used imaging modality to characterize glioblastoma and guide treatments. However, multiparametric imaging is most appropriate to assess biological tumor heterogeneity and more specifically, to quantitatively analyze these three compartments together.

Specific imaging markers of tumor activity have emerged recently, providing additional specific information to further characterize the tumor and its environment (*18*,*19*). In the field of neuro-

oncology, these markers include those derived from multiparametric MRI such as perfusion, diffusion and magnetic resonance spectroscopy. For PET imaging, radiotracers reflecting cell proliferation as ^{18}F-3'-deoxy-3'-^{18}F-fluorothymidine (^{18}F-FLT) (*13*,*20*,*21*), but also amino acid tracers as ^{11}C-Methionine, O-(2-^{18}F-fluoroethyl)-l-tyrosine (^{18}F-FET), or 3,4-dihydroxy-6-^{18}F-fluoro-l-phenylalanine (^{18}F-FDOPA) (*22*) that can specifically differentiate true tumor boundaries from equivocal lesions based and the degree of hypoxia as ^{18}F-fluoromisonidazole (^{18}F-FMISO) (*10*,*12*,*23*), have emerged as the most pertinent for this tumor type.

However, to the best of our knowledge, a spatial analysis of these three parameters, i.e., proliferation, hypervascularization and hypoxia has never been reported using noninvasive imaging for newly diagnosed glioblastoma and only a few papers have performed such characterization in other tumor location (*24*,*25*). Interestingly, the most proliferative, vascularized and hypoxic sub-volumes (i.e. “hotspots”) could also represent regions of high risk of relapse and consequently their identification is of real interest to overcome resistance to therapies such as surgery or radiation therapy.

Therefore, in this study, we aimed to spatially evaluate the volumes and the hotspots of proliferation, hypervascularization and hypoxia, by using ^{18}F-FLT PET, relative Cerebral Blood Volume (rCBV)-MRI and ^{18}F-FMISO PET respectively, relative to CE volume in preoperative glioblastoma patients.

MATERIALS AND METHODS

Patients

Patients with *de novo* glioblastoma were included from two prospective clinical trials funded by INCA (Institut National du Cancer) and approved by the local ethics committee and AFSSAPS agreement (ClinicalTrials.gov identifier: NCT00850278 and NCT01200134). Thirty one patients were included in the Caen University Hospital based on inclusion criteria: presenting histopathologically proven grade IV gliomas based on WHO criteria; eligible in the final analysis with MR and PET imaging modalities, age ≥18 years, KPS ≥50, normal blood cell count, normal biological hepatic functions and a signed informed consent for a voluntary participation in research. Patients underwent ^{18}F-FLT-PET (n=20) and/or ^{18}F-FMISO-PET (n=20) and multiparametric MRI (n=31)(Table 1) within the same week and prior to surgery. Thereafter, patients underwent surgery, resection or biopsy depending on the location of the tumor, and the specimens were histopathologically evaluated by an experienced neuropathologist (ELZ) and only patients with established diagnosis of glioblastoma were analyzed.

Image Acquisition

MR Imaging was performed on a 1.5 Tesla GEMS version HDXt 15.0. After scout-view and coronal T2-weighted imaging, an axial FLAIR (Fluid Attenuated Inversion Recovery) sequence was performed (24 slices, slice spacing 5.5 mm, pixel resolution 0.47×0.47 mm, TR/TE=9 602/150 ms). For DSC-MRI, a dynamic gradient-echo T2*-weighted EPI images was used (14 slices**,** 35 repetitions, slice spacing: 7 mm, pixel resolution 2.19×2.19 mm, TR/TE=2 280/60 ms) to track a bolus of 0.1 mmol/kg of Gadolinium-DOTA (0.1 mmol/kg, Dotarem, Guerbet). An injection delay of 20 s was applied to obtain an accurate estimate of the baseline signal intensity prior to the arrival of the contrast agent and the acquisition lasted 1min20.

Immediately thereafter, a 3DT1-weighted sequence, 3DT1w-Gd (124 slices, slice spacing 1.5 mm, pixel resolution 1.01×1.01 mm^2, TR/TE=17/3 ms) was performed to evaluate the contrast enhancement.

^{18}F-FLT and ^{18}F-FMISO were both produced by the LDM-TEP group (ISTCT, GIP CYCERON) and synthesized as previously described (*12*,*13*,*26*). Data within a brain-focused field of view were acquired on two consecutive days 40 minutes (^{18}F-FLT) and 2 hours (^{18}F-FMISO) after the intravenous injection of 5 MBq/kg (both tracers) and lasted 10 minutes (^{18}F-FLT, to match a clinically feasible approach) and 20 minutes (^{18}F-FMISO). Acquisitions were performed on a General Electric Discovery VCT 64 PET/CT scanner (CYCERON platform). The CT-based attenuation-corrected PET images were reconstructed with an OSEM 2D algorithm (9 subsets and 2 iterations) and filtered in 3D with a Butterworth filter on 1.95×1.95×3.27 mm voxel size. Standardized uptake values (SUV, g/mL) were calculated using the measured concentration of tissue (counts, kBq/mL) divided by the injected activity in kBq/g of body weight.

Image Analysis

MRI image analysis was performed with in-house macros based on the ImageJ software (*27*). PET analyses were performed with PMOD 3.1® software.

rCBV maps were computed using DSC-MRI. Variations of the T2* signal in the tissue was calculated with in-house macros based on ImageJ software as: $\Delta R_2^*(t) = -1.\ln(S(t)/S_0)$ /TE, with: S_0=signal intensity before contrast agent injection, S(t)= signal intensity over time and TE is Echo time. Then, CBV maps were generated by integrating the area under the γ-variate fitted curves to avoid an effect of recirculation (*28*). Images were then normalized by dividing CBV maps with the mean value of the normal-appearing contralateral side to obtain rCBV maps.

Co-registration: rCBV maps, FLAIR, 3DT1w-Gd and ^{18}F-FMISO PET images were co-registered with trilinear interpolation, rigid matching and normalized mutual information on ^{18}F-FLT PET images (PMOD 3.1® software).

Volume Segmentation: In the present study, we had to tune the segmentation for each imaging modality since none of the various methods we used was considered pertinent enough for the three imaging modalities, which differed in term of contrast/tumor ratio, signal intensity. Also, we paid attention to the accuracy of the segmentation modality for all patients in one imaging modality. When two methods were almost similar, and to avoid any over-interpretation of our results, the most restrictive one was retained.

Volume Segmentation For ^{18}F-FLT PET: The visual inspection easily enabled us to eliminate 40% SUV max, which underestimates volume, whereas Mean Contra + 3.3SD overestimates volume (Supplementary Fig.1). A semi-automated algorithm previously validated for ^{18}F-FLT PET images named FLAB -Fuzzy Locally Adaptive Bayesian- was exploited, using 2 or 3 classes (*29*–*33*).

Volume Segmentation For ^{18}F-FMISO PET: We considered FLAB, 1.2 T/B (Tissue/Blood), 40% SUVmax and Mean Contra + 3.3SD, and compared them to each other quantitatively as well as through visual inspection.

As exemplified in Supplementary Fig. 2, the standard 1.2 T/B segmentation failed for some cases. For 40% of SUVmax, it was visually striking that an overestimation of hypoxic volumes occurred. We then performed either FLAB segmentation or a semi-automated segmentation using a statistical approached based on the Mean Contra + 3.3 SD (*34*). As compared to T/B approach, we believe this segmentation could be very well suited in the routine situation because it does not require to draw and process radioactive blood. Thus, with the exception of a few pixels

removed by hiding with FLAIR hypersignal, no further manual intervention was necessary, making this technique particularly well suited. This statistical approach, Mean Contra + 3.3 SD, seems suitable for a tracer like FMISO with an average uptake and a large standard deviation in the healthy brain parenchyma and a poor tumor/contralateral contrast.

FLAB and Mean Contra +3.3 SD led to very similar results (Supplementary Fig. 2). In some cases, FLAB provided slightly larger hypoxic volumes than Mean Contra + 3.3 SD; we retained the less permissive strategy.

Volume Segmentation For CBV: The situation relates to FMISO situation since a blood volume is present in the healthy brain tissue, the statistical approach resulted in accurate segmentation compared to the naked eyes. We used an already published methodology (*35*) assuming a threshold at 2 or 3 greater than the signal of the Normal Appearing White Matter (NAWM). We also compared to a contralateral ROI composed of both grey and white matter with a threshold at Mean Contra + 1.96 SD. For both methods, only the region included into the FLAIR region were retained. The two methods provided very similar results but Mean Contra + 1.96 SD was less permissive (Supplementary Fig.3).

Hotspot Segmentation: For each modality, the hotspot area was defined as the 95^{th} centile of histogram distribution in the 3D-ROI defined on FLAIR hypersignal to include all voxels that may extend to gadolinium (Gd) enhancement ROI.

All segmented areas were then used as 3D-ROI for further studies.

Peripheral Volume And Hotspot Calculation: After the segmentation process, for each modality and each patient, we defined a peripheral volume and peripheral hotspot as the percentage of

the ROI of the modality of interest that is outside the volume of CE using a Boolean operation. This volume was calculated using the following equations.

$$Peripheral\ volume(\%) = \frac{ROI\ of\ thev\ olume\ of\ the\ modality\ NOT\ ROI\ of\ CE}{ROI\ of\ CE} * 100$$

$$Peripheral\ hotspot(\%) = \frac{ROI\ of\ the\ hot\ spot\ of\ the\ modality\ NOT\ ROI\ of\ CE}{ROI\ of\ CE} * 100$$

RESULTS

All tumors were confirmed to be a glioblastoma by the pathologist and exhibited a marked CE on 3DT1w-Gd images, elevated rCBV, and pronounced ^{18}F-FLT and ^{18}F-FMISO uptakes. Fig.1 shows representative example of two glioblastoma patients with the multimodal imaging, 3DT1w-Gd, ^{18}F-FLT PET, rCBV maps, ^{18}F-FMISO PET. Based on visual inspection by an expert in PET imaging, a marked intra-tumoral heterogeneity of tracer uptake on both PET images was observed. Since the contrast enhancement is the main target of treatments (surgery; radiation therapy), we then paid attention to the spatial relationship between each modality and CE region.

Analyses of the Peripheral Volume Outside the Contrast Enhancement Region

Thresholded regions of proliferation with ^{18}F-FLT, of hypervascularization with rCBV and of hypoxia with ^{18}F-FMISO (Fig. 2 top) were overlaid on the T1w-Gd images (Fig. 2 bottom). Fig. 2 and the peripheral volume calculated (Fig. 3, patient #20) illustrated that the volume of FLT uptake extended far from CE area (139%). The similar situation also occurs for FMISO uptake, but less pronounced where the peripheral volume was 43%, while for CBV, only 11% of the segmented area extended in the non-enhancing area. A representative example of the three modalities segmentation overlayed on the T1w-Gd is provided (Supplementary Fig.4).

The peripheral volume outside CE volume calculated for each patient (Fig. 3) clearly demonstrated that extension of metabolic areas beyond the CE volume was highly variable. The range of peripheral volumes for ^{18}F-FLT, rCBV and ^{18}F-FMISO were respectively [1.6 - 155.5 %], [1.5 – 89.5%] and [3.1 - 78.0%]. More precisely, over the 20 patients investigated with FLT, 9/20 had a % comprised between 0 and 20%; 5/20 between 20 and 40 % but 6/20 had % of peripheral volume greater than 40%. For CBV, 17/31 had a % comprised between 0 and 20%; 10/31 between 20 and

40 % but 4/31 had % of peripheral volume greater than 40%. For ^{18}F-FMISO, 10/20 had a value comprised between 0 and 20%; 7/20 between 20 and 40 % but 3/20 had % of peripheral volume greater than 40%.

Analyses of the Peripheral Hotspots Outside the Contrast Enhancement Region

Considering the strong intra-tumor heterogeneity observed on multiparametric imaging, we were interested in further identifying sub-volumes in the tumor that could be likely associated with resistance and early recurrence. Hyper-proliferative, hypervascularized and severe hypoxic hotspots were thresholded (Fig. 4, top) and overlaid on the T1w-Gd images (Fig. 4, bottom). In this example, a percentage of the hyperproliferative (18%), the hypervascular (11%) and the most hypoxic region (3%) were located outside the CE region.

The peripheral hotspots outside CE volume were calculated for each patient (Fig. 5) and showed that all patients had hyperproliferative volume outside CE volume [8.8 – 32.5 %]. More precisely, 1/20 had less than 10%, 15/20 had values comprised between 10 and 20%, and 4/20 between 20 and 40 %. Concerning hypervascularized hotspots [0 – 25.2%], in 23/31 patients the hotspot fraction less than 5%, 7/31 had a value comprised between 5 and 20% and in 1/31 it was 25%. Last, most hypoxic area was mainly detected in the enhancement region [0 – 5.7%], since 14/20 patients had less than 1% of the FMISO hotspot outside the CE volume, and the others around 5%.

DISCUSSION

In the context of glioblastoma, intertumoral and intratumoral heterogeneity has been attributed to the failure of standardized treatments. Among the factors influencing tumor growth, the study of the *in vivo* relationship between proliferation, angiogenesis and hypoxia remains of

great interest relative to the conventional aggressive region defined on contrast enhancement MRI. In the context of glioblastoma, the present study is the first one to show spatial distribution of each modality together and relative to contrast enhancement.

In the literature and based on multivariate analyses, it has been shown that each parameter was independently associated with the tumor volume (*17*,*26*,*36*). In gliomas, elevated ^{18}F-FLT uptake has been shown to be correlated with Ki67 immunostaining expression and to reflect proliferation (*37*–*39*). In gliomas also, high hypoxia has been shown to be a poor prognosis factor (*40*).

As exemplified on Fig. 1, our results confirm that all three analyzed parameters are interlinked and that an increase of each parameter occurs concomitantly (*9*,*11*). Increased rCBV along with hypoxia might indicate tumor-induced angiogenesis to counteract changes in oxygenation that occur along with the metabolic demand of proliferating cells.

Following a visual inspection, each modality on Fig. 1 clearly showed a variable uptake distribution that would need to be exploited. As previously published (*9*,*10*,*17*), it confirms that the heterogeneity can be mapped using multimodal imaging.

However, our results on peripheral volume also showed that active tumor tissues were already present in areas that could be considered as non-pathologic according to contrast enhancement on MRI, and which therefore might not be targeted by the treatment. This is especially true for ^{18}F-FLT PET, which clearly showed that proliferating cells extended outside the enhancement region on T1w-Gd images, as shown in earlier publications (*36*).

One of our main results is that FLT PET volume was greater than the other volumes. The spatial analysis shows that ^{18}F-FLT volume encompasses the rCBV, contrast enhancement and the ^{18}F-

FMISO volume for the most patients. This result is in line with those already published, which also demonstrated that in most cases, ^{18}F-FLT uptake was larger than tumor volume assessed by anatomical MRI. In glioma, elevated ^{18}F-FLT uptake is correlated with Ki67 and reflects proliferation (*37*,*38*). This result strengthens the hypothesis that the tumoral proliferation is the driving force of the other parameters analyzed in this study, namely angiogenesis and hypoxia.

Various papers have discussed the dependency of FLT uptake to the integrity of the BBB see for review (*41*). It is recognized that a major limiting factor of ^{18}F-FLT uptake is the transport mechanism and leakage via the disrupted blood-tumor barrier could result in increased uptake. In a recent paper from Watkins et al. (*42*), they suggest that only a small number of glioma cells could be sufficient to damage the integrity of the BBB which might explain the ability of FLT to detect proliferating cells in non-enhancing regions of the tumor.

The hotspots analysis showed that all tumors had hyperproliferative area that extended outside the CE volume, while hypervascularized or severe hypoxic areas were mostly included within the CE volume. This result concurs with a recent publication using ^{11}C-Methionine and demonstrating the presence of metabolic tumor volume following gross tumor resection (*43*).

These results strengthen the fact that tumor cells have already infiltrated the non-enhancing tissue and ought to be included in the surgical treatment or in the definition of the Biological Target Volume for radiotherapy (*43*).

Nowadays, the standard surgical treatment of glioblastoma is the removal of CE area (*44*). As we showed that metabolically active areas are visible outside the enhancement volume, removal of the CE volume could contribute in explaining a rapid recurrence of glioblastoma. We suggest to

resect glioblastoma beyond CE volume and until functional limits while preserving the quality of life (*45*). This information may also be used as a parameter for improving the accuracy of the biopsy analysis and if biopsy and imaging concur, it could be used to improve the quality of resection.

This information contributes to the definition of gross target volumes for radiotherapy, integrating these findings in the concept of Biological Target Volume (*46*). This could lead to a better tumor control, as it is known that the majority of relapses occurs within the irradiation field (*47*,*48*), illustrating the radiation resistance of some areas within the irradiated volume. It is assumed that the current radiotherapy regimen does not guarantee the curative doses necessary to counteract radioresistance of some areas of the tumor identified as hotspots in this paper and which may contribute to the failure of the conventional treatments (*49*). Radiotherapy is likely to be optimized by specifically targeting these unfavorable biological characteristics (*49*,*50*).

This study has some limitations. We only studied each modality with respect to T1 enhancement and we did not perform voxel-wise analyses between the various modalities. However, the main goal of the present analysis was to make a study as simple as possible relative to T1 enhancement that could provide useful information to the physician at the individual level to adapt or tune therapeutic strategies. Also the use of other PET tracers such as amino acid tracers (^{11}C-Met; ^{18}F-FET; ^{18}F-FDOPA) might also provide very accurate information in mapping region potentially involved in tumor recurrence. For the hot spot-study, given the method of calculation for each patient, a potential overinterpretation of low activity could occur. As a consequence comparison of our results to include the peripheral volumes or the hot-spot in the therapeutic strategies to stereotaxic biopsies would also be of great importance. We are now

incorporating this strategy in ongoing clinical trials.

CONCLUSION

Even if it is difficult to draw a general overview for each individual patient, this study underlines the complementary value of using different multiparametric imaging to assess tumor heterogeneity, and to define tumor volume and sub volumes that are likely to be resistant to conventional therapies.

DISCLOSURE

Authors declare that they have no conflict of interest.

ACKNOWLEDGEMENTS

Conseil Régional de Normandie, Elen Fund, Institut National du Cancer (grant #RECF1475), Agence Nationale de la Recherche-Labex IRON (ANR-11-LABX-0018–01). We are grateful for Dr Aurélien Corroyer-Dulmont for his helpful comments.

KEY POINTS

QUESTION: Identify the spatial relationship between proliferation, vascularization and hypoxia in preoperative glioblastoma patients, with respect to the contrast enhancement area on T1w-Gd images.

PERTINENT FINDINGS: Clinical trials demonstrating the heterogeneity of the three parameters measured, namely proliferation, vasculature and hypoxia over the classically used contrast-enhancement.

IMPLICATIONS FOR PATIENT CARE: This study clearly demonstrates the significance of incorporating more functional parameters for patient management.

REFERENCES

1. Stupp R, Hegi ME, Mason WP, et al. Effects of radiotherapy with concomitant and adjuvant temozolomide versus radiotherapy alone on survival in glioblastoma in a randomised phase III study: 5-year analysis of the EORTC-NCIC trial. *Lancet Oncol*. 2009;10:459-466.

2. Wen PY, Weller M, Lee EQ, et al. Glioblastoma in adults: A Society for Neuro-Oncology (SNO) and European Society of Neuro-Oncology (EANO) consensus review on current management and future directions. *Neuro-Oncol*. 2020; 22:1073-1113.

3. Louis DN, Perry A, Reifenberger G, et al. The 2016 World Health Organization classification of tumors of the central nervous system: a summary. *Acta Neuropathol (Berl)*. 2016;131:803-820.

4. Verhaak RGW, Hoadley KA, Purdom E, et al. Integrated genomic analysis identifies clinically relevant subtypes of glioblastoma characterized by abnormalities in PDGFRA, IDH1, EGFR, and NF1. *Cancer Cell*. 2010;17:98-110.

5. Bergmann N, Delbridge C, Gempt J, et al. The intratumoral heterogeneity reflects the intertumoral subtypes of glioblastoma multiforme: a regional immunohistochemistry analysis. *Front Oncol*. 2020;10:494.

6. Li C, Wang S, Yan J-L, et al. Intratumoral heterogeneity of glioblastoma infiltration revealed by joint histogram analysis of diffusion tensor imaging. *Neurosurgery*. 2019;85:524-534.

7. Chinot OL, Wick W, Mason W, et al. Bevacizumab plus radiotherapy-temozolomide for newly diagnosed glioblastoma. *N Engl J Med*. 2014;370:709-722.

8. Swanson KR, Bridge C, Murray JD, Alvord EC. Virtual and real brain tumors: using mathematical modeling to quantify glioma growth and invasion. *J Neurol Sci*. 2003;216:1-10.

9. Evans SM, Jenkins KW, Chen HI, et al. The relationship among hypoxia, proliferation, and outcome in patients with de novo glioblastoma: a pilot study. *Transl Oncol*. 2010;3:160-169.

10. Gerstner E, Zhang Z, Fink J, et al. ACRIN 6684: Assessment of tumor hypoxia in newly diagnosed GBM using 18F-FMISO PET and MRI. *Clin Cancer Res*. 2016;22:5079-5086.

11. Swanson KR, Rockne RC, Claridge J, Chaplain MA, Alvord EC, Anderson ARA. Quantifying the role of angiogenesis in malignant progression of gliomas: in silico modeling integrates imaging and histology. *Cancer Res*. 2011;71:7366-7375.

12. Bekaert L, Valable S, Lechapt-Zalcman E, et al. [18F]-FMISO PET study of hypoxia in gliomas before surgery: correlation with molecular markers of hypoxia and angiogenesis. *Eur J Nucl Med Mol Imaging*. 2017;44:1383-1392.

13. Collet S, Valable S, Constans JM, et al. [(18)F]-fluoro-l-thymidine PET and advanced MRI for preoperative grading of gliomas. *NeuroImage Clin*. 2015;8:448-454.

14. Fernandez P, Zanotti-Fregonara P, Eimer S, et al. Combining 3'-Deoxy-3'-[18F] fluorothymidine and MRI increases the sensitivity of glioma volume detection. *Nucl Med Commun*. 2019;40:1066-1071.

15. Leimgruber A, Hickson K, Lee ST, et al. Spatial and quantitative mapping of glycolysis and hypoxia in glioblastoma as a predictor of radiotherapy response and sites of relapse. *Eur J Nucl Med Mol Imaging*. 2020;47:1476-1485.

16. Ponte KF da, Berro DH, Collet S, et al. In vivo relationship between hypoxia and angiogenesis in human glioblastoma: a multimodal imaging study. *J Nucl Med*. 2017;58:1574-1579.

17. Szeto MD, Chakraborty G, Hadley J, et al. Quantitative metrics of net proliferation and invasion link biological aggressiveness assessed by MRI with hypoxia assessed by FMISO-PET in newly diagnosed glioblastomas. *Cancer Res*. 2009;69:4502-4509.

18. Kickingereder P, Radbruch A, Burth S, et al. MR perfusion-derived hemodynamic parametric response mapping of bevacizumab efficacy in recurrent glioblastoma. *Radiology*. 2016;279:542-552.

19. Miyake K, Shinomiya A, Okada M, Hatakeyama T, Kawai N, Tamiya T. Usefulness of FDG, MET and FLT-PET studies for the management of human gliomas. *J Biomed Biotechnol*. 2012;2012:205818.

20. Berro DH, Collet S, Constans J-M, et al. Comparison between MRI-derived ADC maps and 18FLT-PET in pre-operative glioblastoma. *J Neuroradiol*. 2019;46:359-366.

21. Brahm CG, den Hollander MW, Enting RH, et al. Serial FLT PET imaging to discriminate between true progression and pseudoprogression in patients with newly diagnosed glioblastoma: a long-term follow-up study. *Eur J Nucl Med Mol Imaging*. 2018;45:2404-2412.

22. Najjar AM, Johnson JM, Schellingerhout D. The emerging role of amino acid PET in neuro-oncology. *Bioeng Basel Switz*. 2018;5.

23. Chakhoyan A, Guillamo J-S, Collet S, et al. FMISO-PET-derived brain oxygen tension maps: application to glioblastoma and less aggressive gliomas. *Sci Rep*. 2017;7:10210.

24. van Elmpt W, Zegers CML, Reymen B, et al. Multiparametric imaging of patient and tumour heterogeneity in non-small-cell lung cancer: quantification of tumour hypoxia, metabolism and perfusion. *Eur J Nucl Med Mol Imaging*. 2016;43:240-248.

25. Vera P, Bohn P, Edet-Sanson A, et al. Simultaneous positron emission tomography (PET) assessment of metabolism with ^{18}F-fluoro-2-deoxy-d-glucose (FDG), proliferation with ^{18}F-fluoro-thymidine (FLT), and hypoxia with ^{18}fluoro-misonidazole (F-miso) before and during radiotherapy in patients with non-small-cell lung cancer (NSCLC): a pilot study. *Radiother Oncol*. 2011;98:109-116.

26. Jacobs AH, Thomas A, Kracht LW, et al. 18F-fluoro-L-thymidine and 11C-methylmethionine as markers of increased transport and proliferation in brain tumors. *J Nucl Med.* 2005;46:1948-1958.

27. Schneider CA, Rasband WS, Eliceiri KW. NIH image to imageJ: 25 years of image analysis. *Nat Methods*. 2012;9:671-675.

28. Boxerman JL, Schmainda KM, Weisskoff RM. Relative cerebral blood volume maps corrected for contrast agent extravasation significantly correlate with glioma tumor grade, whereas uncorrected maps do not. *AJNR Am J Neuroradiol*. 2006;27:859-867.

29. Hatt M, Cheze le Rest C, Turzo A, Roux C, Visvikis D. A fuzzy locally adaptive bayesian segmentation approach for volume determination in PET. *IEEE Trans Med Imaging*. 2009;28:881-893.

30. Hatt M, Cheze le Rest C, Descourt P, et al. Accurate automatic delineation of heterogeneous functional volumes in positron emission tomography for oncology applications. *Int J Radiat Oncol Biol Phys*. 2010;77:301-308.

31. Arens AIJ, Troost EGC, Hoeben BAW, et al. Semiautomatic methods for segmentation of the proliferative tumour volume on sequential FLT PET/CT images in head and neck carcinomas and their relation to clinical outcome. *Eur J Nucl Med Mol Imaging*. 2014;41:915-924.

32. Hatt M, Laurent B, Ouahabi A, et al. The first MICCAI challenge on PET tumor segmentation. Med Image Anal. 2018 Feb;44:177-195

33. Hatt M, Lee JA, Schmidtlein CR, et al. Classification and evaluation strategies of auto-segmentation approaches for PET: Report of AAPM task group No. 211. Med Phys. 2017 Jun;44(6):e1-e42.

34. Henriques de Figueiredo B, Zacharatou C, Galland-Girodet S, et al. Hypoxia imaging with [18F]-FMISO-PET for guided dose escalation with intensity-modulated radiotherapy in head-and-neck cancers. *Strahlenther Onkol*. 2015;191:217-224.

35. Crawford FW, Khayal IS, McGue C, et al. Relationship of pre-surgery metabolic and physiological MR imaging parameters to survival for patients with untreated GBM. *J Neurooncol*. 2009;91:337-351.

36. Kawai N, Maeda Y, Kudomi N, et al. Correlation of biological aggressiveness assessed by 11C-methionine PET and hypoxic burden assessed by 18F-fluoromisonidazole PET in newly diagnosed glioblastoma. *Eur J Nucl Med Mol Imaging*. 2011;38:441-450.

37. Corroyer-Dulmont A, Pérès EA, Petit E, et al. Detection of glioblastoma response to temozolomide combined with bevacizumab based on µMRI and µPET imaging reveals [18F]-fluoro-L-thymidine as an early and robust predictive marker for treatment efficacy. *Neuro-Oncol*. 2013;15:41-56.

38. Ullrich R, Backes H, Li H, et al. Glioma proliferation as assessed by 3'-fluoro-3'-deoxy-L-thymidine positron emission tomography in patients with newly diagnosed high-grade glioma. *Clin Cancer Res*. 2008;14:2049-2055.

39. Viel T, Talasila KM, Monfared P, et al. Analysis of the growth dynamics of angiogenesis-dependent and -independent experimental glioblastomas by multimodal small-animal PET and MRI. *J Nucl Med*. 2012;53:1135-1145.

40. Spence AM, Muzi M, Swanson KR, et al. Regional hypoxia in glioblastoma multiforme quantified with [18F]fluoromisonidazole positron emission tomography before radiotherapy: correlation with time to progression and survival. *Clin Cancer Res*. 2008;14:2623-2630.

41. Nikaki A, Angelidis G, Efthimiadou R, et al. 18F-fluorothymidine PET imaging in gliomas: an update. *Ann Nucl Med*. 2017;31:495-505.

42. Watkins S, Robel S, Kimbrough IF, Robert SM, Ellis-Davies G, Sontheimer H. Disruption of astrocyte-vascular coupling and the blood-brain barrier by invading glioma cells. *Nat Commun*. 2014;5:4196.

43. Miller S, Li P, Schipper M, et al. Metabolic tumor volume response assessment using (11)C-methionine positron emission tomography identifies glioblastoma tumor subregions that predict progression better than baseline or anatomic magnetic resonance imaging alone. *Adv Radiat Oncol*. 2020;5:53-61.

44. D'Amico RS, Englander ZK, Canoll P, Bruce JN. Extent of resection in glioma-a review of the cutting edge. *World Neurosurg*. 2017;103:538-549.

45. Duffau H. Surgery for malignant brain gliomas: fluorescence-guided resection or functional-based resection? *Front Surg*. 2019;6:21.

46. Ling CC, Humm J, Larson S, et al. Towards multidimensional radiotherapy (MD-CRT): biological imaging and biological conformality. *Int J Radiat Oncol Biol Phys*. 2000;47:551-560.

47. Ghose A, Lim G, Husain S. Treatment for glioblastoma multiforme: current guidelines and canadian practice. *Curr Oncol Tor Ont*. 2010;17:52-58.

48. Milano MT, Okunieff P, Donatello RS, et al. Patterns and timing of recurrence after temozolomide-based chemoradiation for glioblastoma. *Int J Radiat Oncol Biol Phys*. 2010;78:1147-1155.

49. Gérard M, Corroyer-Dulmont A, Lesueur P, et al. Hypoxia imaging and adaptive radiotherapy: a state-of-the-art approach in the management of glioma. *Front Med*. 2019;6:117.

50. Piroth MD, Pinkawa M, Holy R, et al. Integrated boost IMRT with FET-PET-adapted local dose escalation in glioblastomas. Results of a prospective phase II study. *Strahlenther Onkoll*. 2012;188:334-339.

Table 1: flowchart of the study (patients were followed by 18F-FLT PET along with MRI and/or by 18F-FMISO PET along with MRI)

	"FLT" study		
	"Hyponco" study		
Patient #	**^{18}F-FLT PET**	**rCBV MRI**	**^{18}F-FMISO PET**
2	✓	✓	
3	✓	✓	
4	✓	✓	
5	✓	✓	
6	✓	✓	
7	✓	✓	
8	✓	✓	
9	✓	✓	
10	✓	✓	✓
11	✓	✓	✓
12	✓	✓	
13	✓	✓	
14	✓	✓	✓
15		✓	✓
16	✓	✓	✓
17	✓	✓	✓
18	✓	✓	✓
19	✓	✓	✓
20	✓	✓	✓
21	✓	✓	✓
22		✓	✓
23		✓	✓
24		✓	✓
25		✓	✓
26		✓	✓
27		✓	✓
28		✓	✓
29		✓	✓
30		✓	✓
31		✓	✓

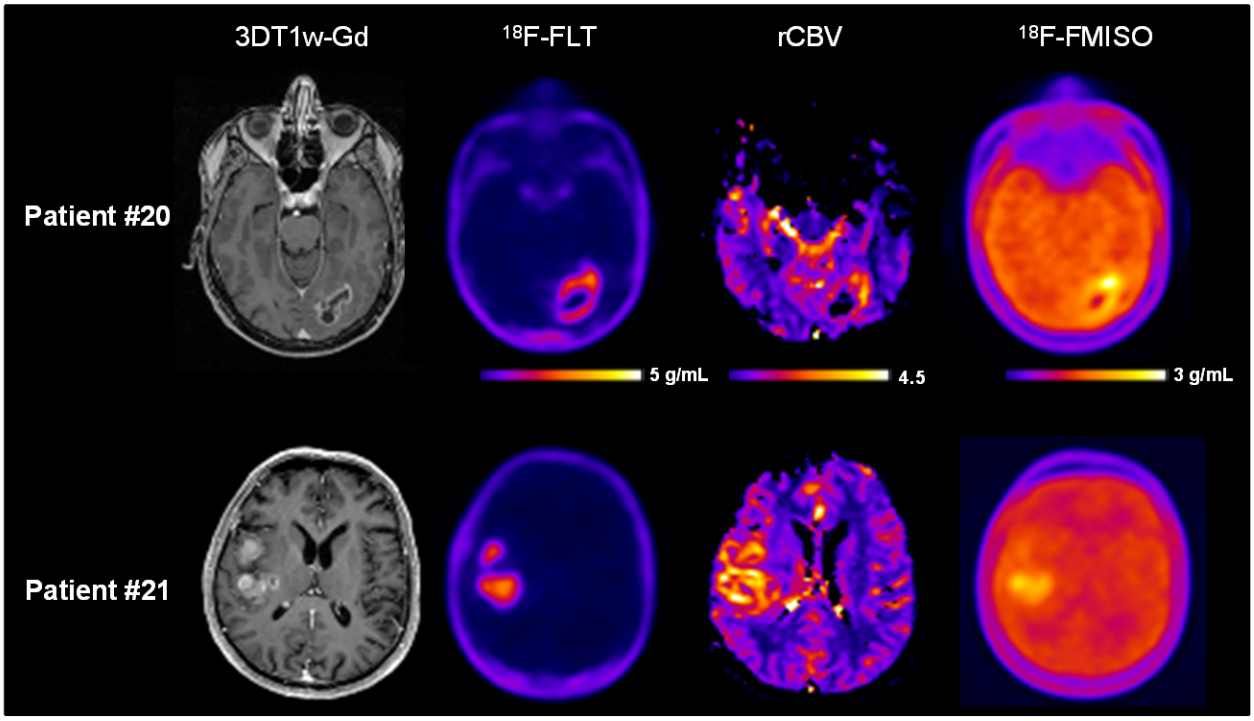

Figure 1: multimodal imaging of two glioblastoma patients with 3DT1w-Gd, ^{18}F-FLT PET, rCBV MRI and ^{18}F-FMISO PET.

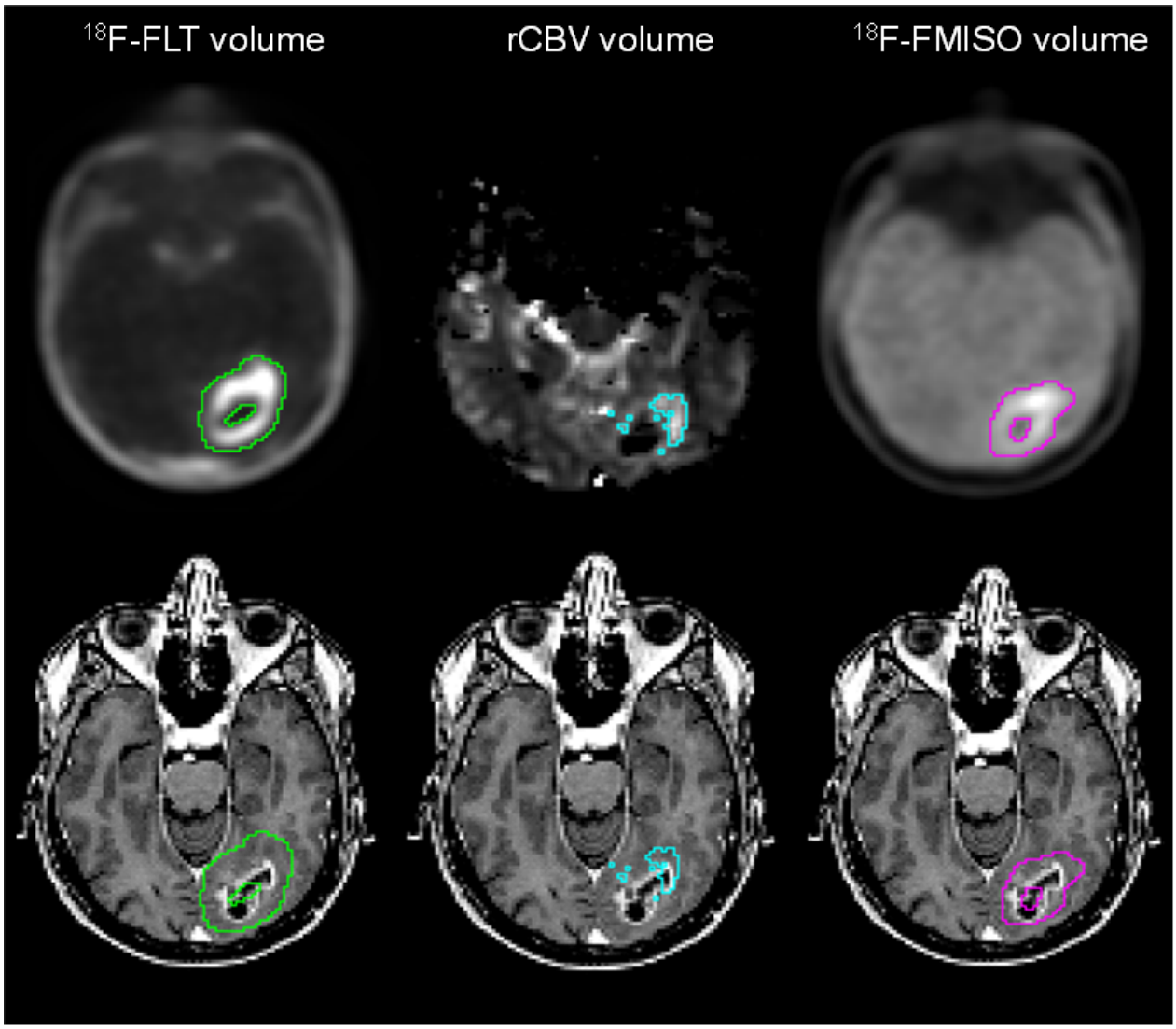

Figure 2: example of proliferative volume in green, hypervascularized volume in blue and hypoxic volume in pink segmented (top) and overlaid 3DT1w-Gd image (bottom).

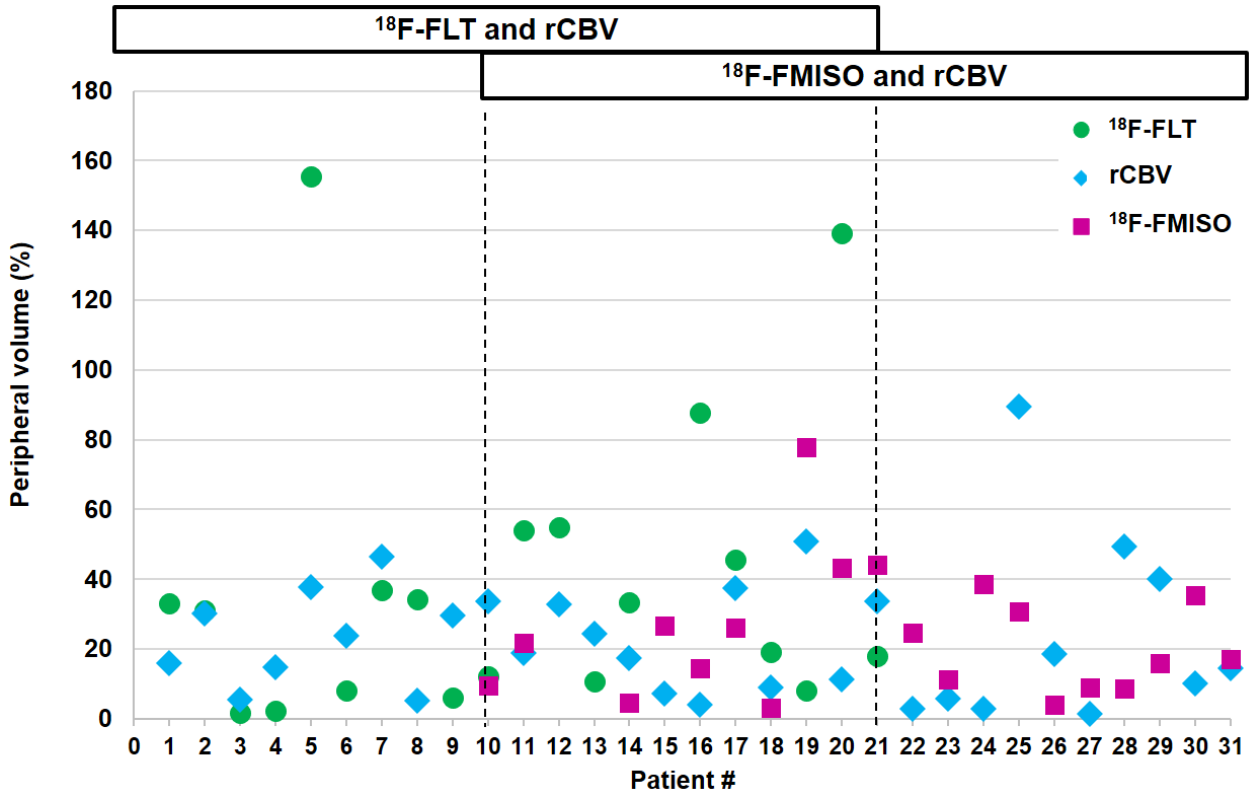

Figure 3: percentage of peripheral volume of ^{18}F-FLT, rCBV and ^{18}F-FMISO outside contrast enhancement volume.

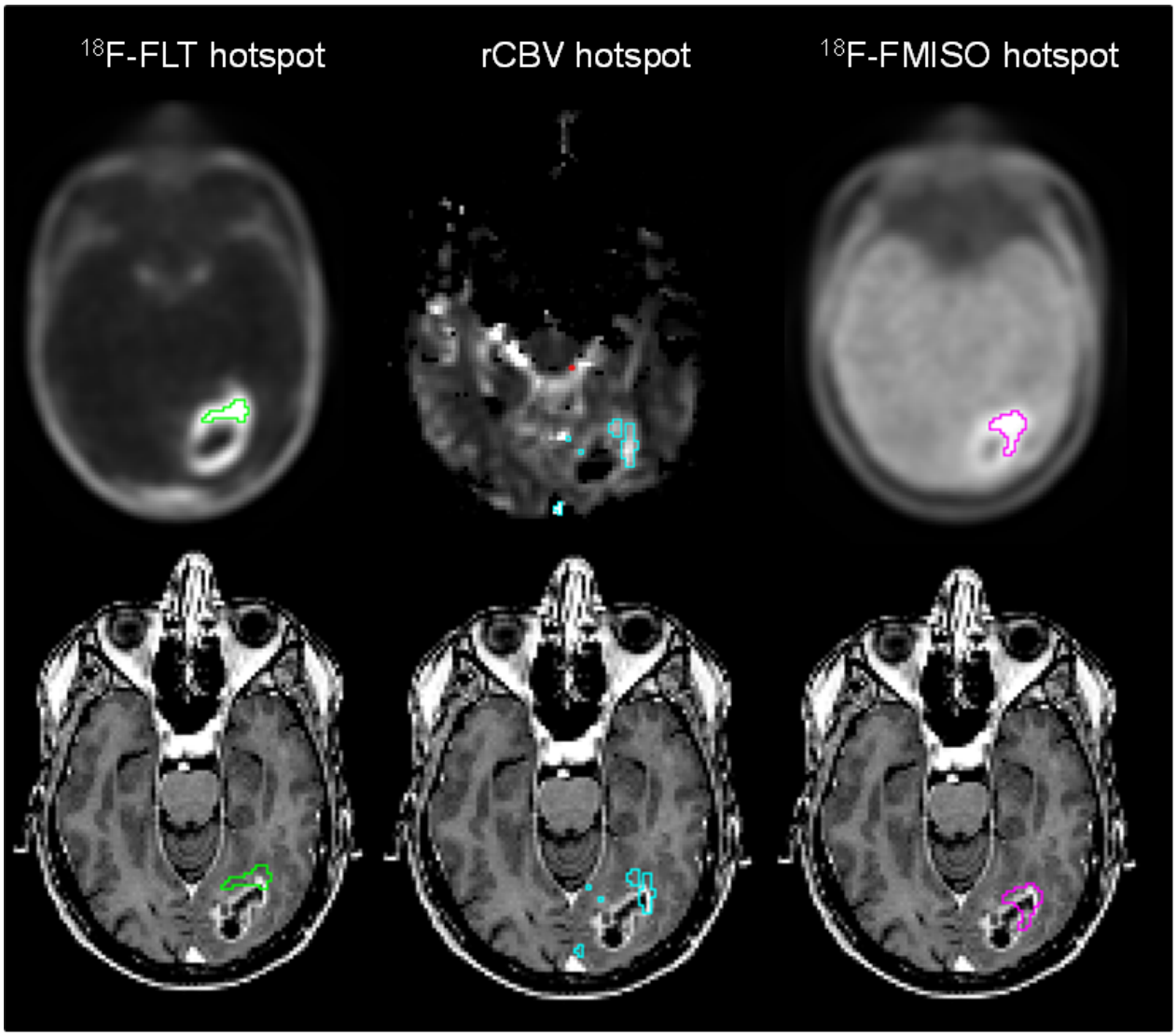

Figure 4: example of proliferative hotspot (in green), hypervascularized hotspot (in blue) and hypoxic hotspot (in pink) segmented (top) and overlaid on T1w-Gd image (bottom).

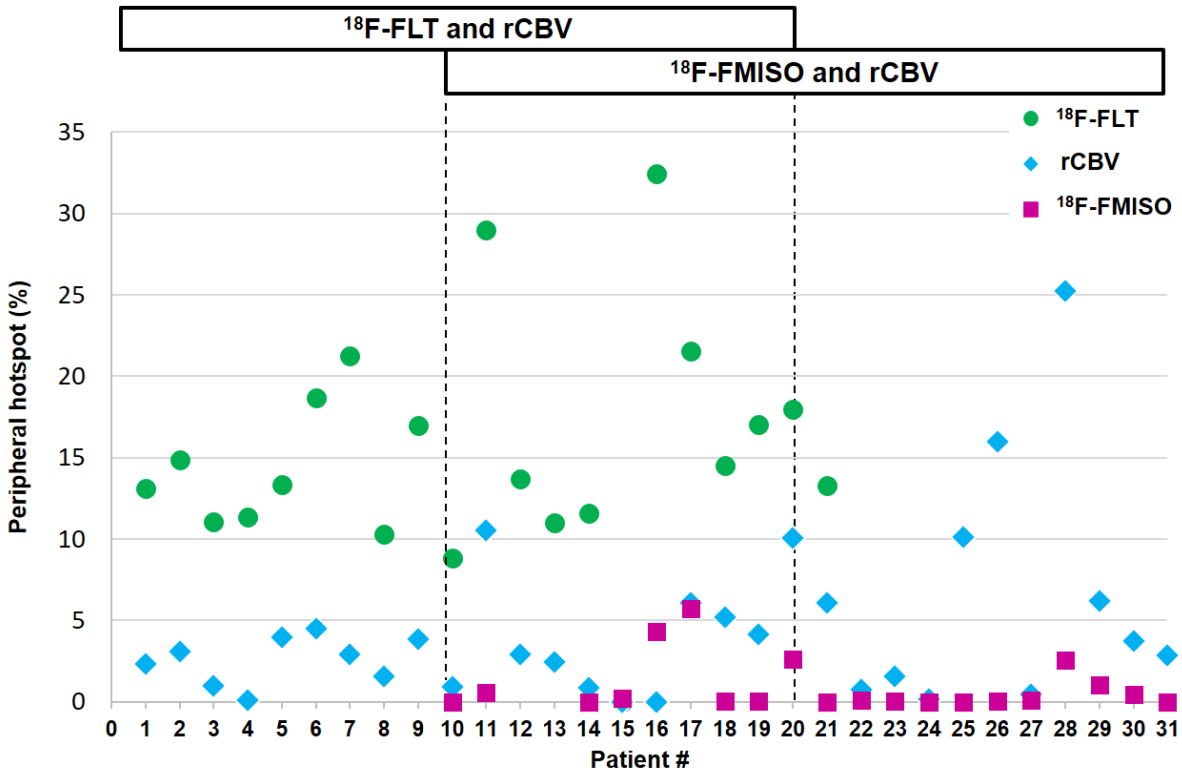

Figure 5: percentage of peripheral hotspots volume of ^{18}F-FLT, rCBV and ^{18}F-FMISO outside contrast enhancement (CE).

Graphical Abstract

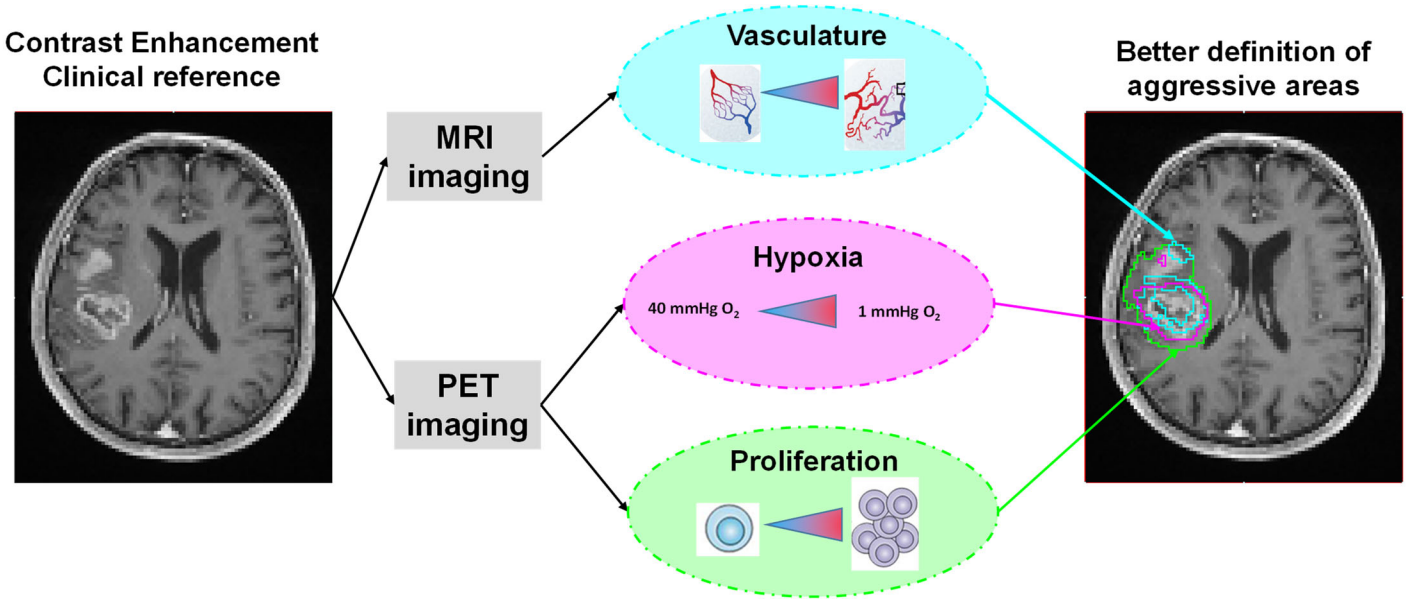

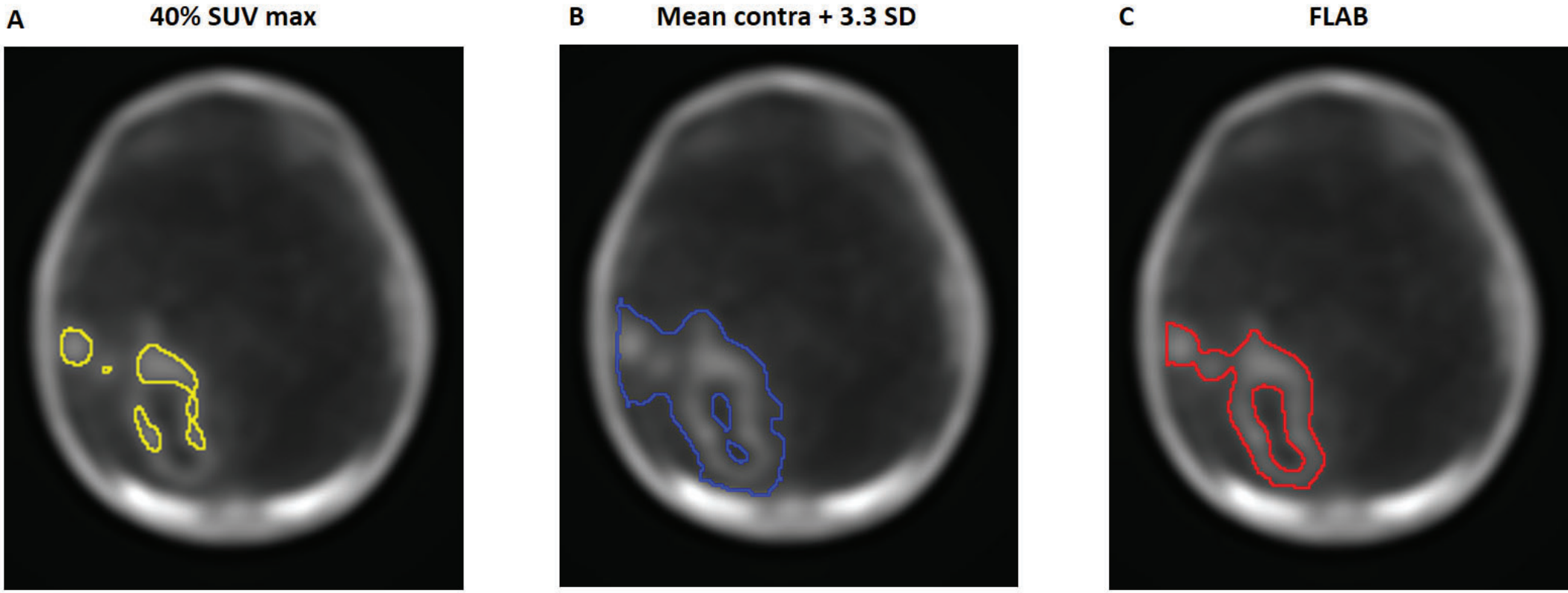

Supplemental Figure 1: Representative example of the various segmentation methodologies used for FLT images.
Panel A represents 40% of SUV max segmentation (yellow ROI) overlaid on FLT image, panel B represents Mean Contralateral + 3.3 SD (blue ROI) overlaid on FLT image. Panel C represents FLAB (red ROI) overlaid on FLT image.

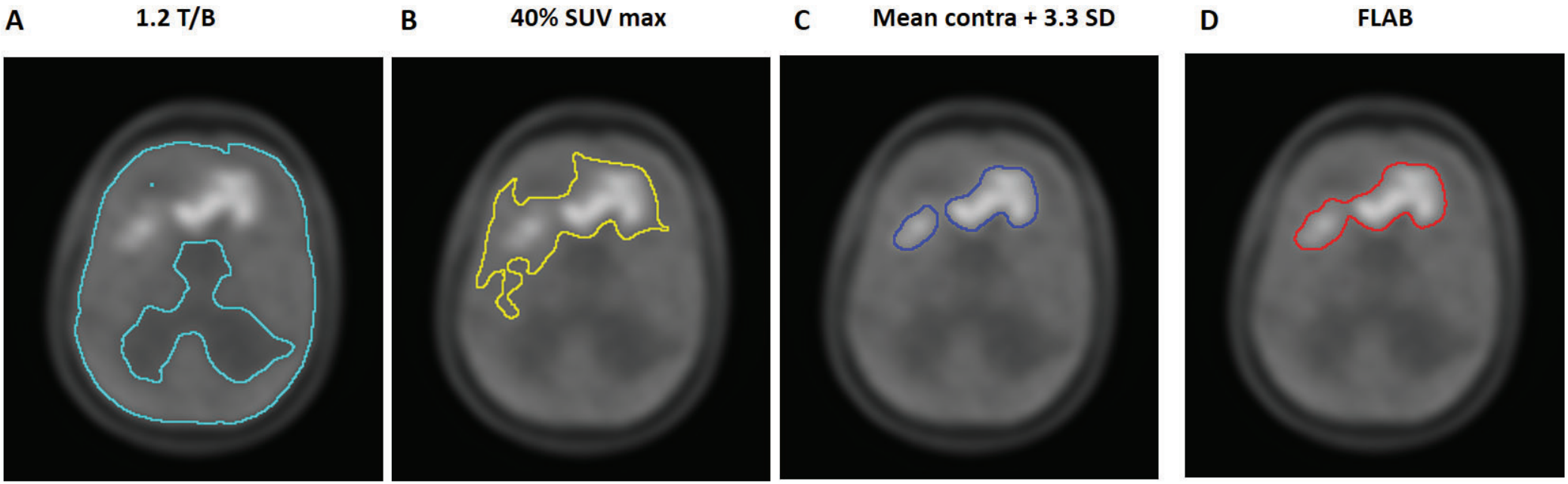

Supplemental Figure 2: Representative examples of the various segmentation methodologies used for FMISO images.
Panel A represents 1.2 T/B segmentation (cyan ROI) overlaid on FMISO image. Panel B represents 40% of SUV max segmentation (yellow ROI) overlaid on FMISO image. Panel C represents mean Contralateral + 3.3 SD (blue ROI) overlaid on FMISO image. Panel D represents FLAB (red ROI) overlaid on FMISO image

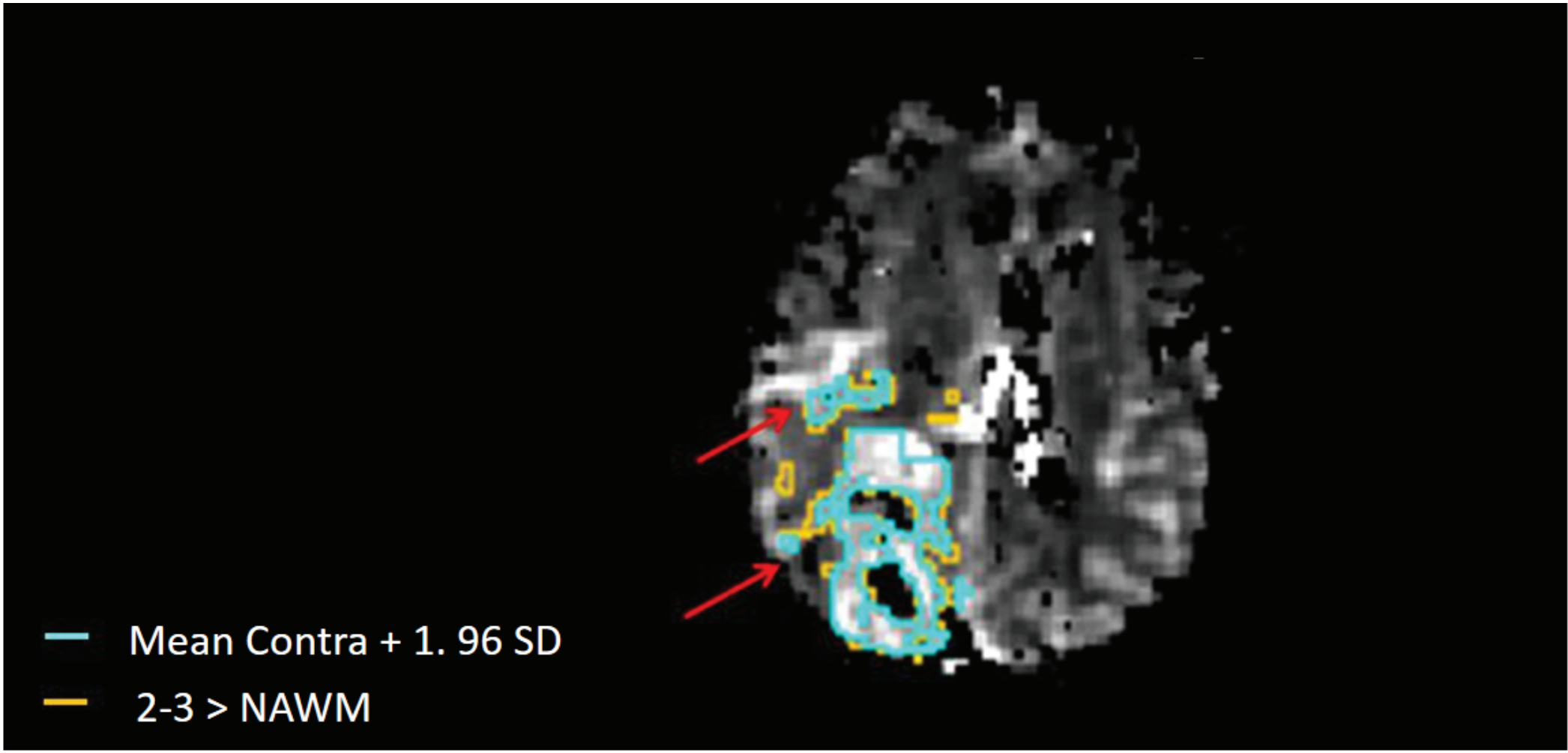

Supplemental Figure 3: Representative examples of the two segmentation strategies used for rCBV segmentation. Yellow overlay represents a threshold at 2-3 time greater than NAWM and the Cyan overlay represents a mean contralateral +1.96 SD. Arrows refer to suspicious regions that are excluded after masking with the FLAIR ROI.

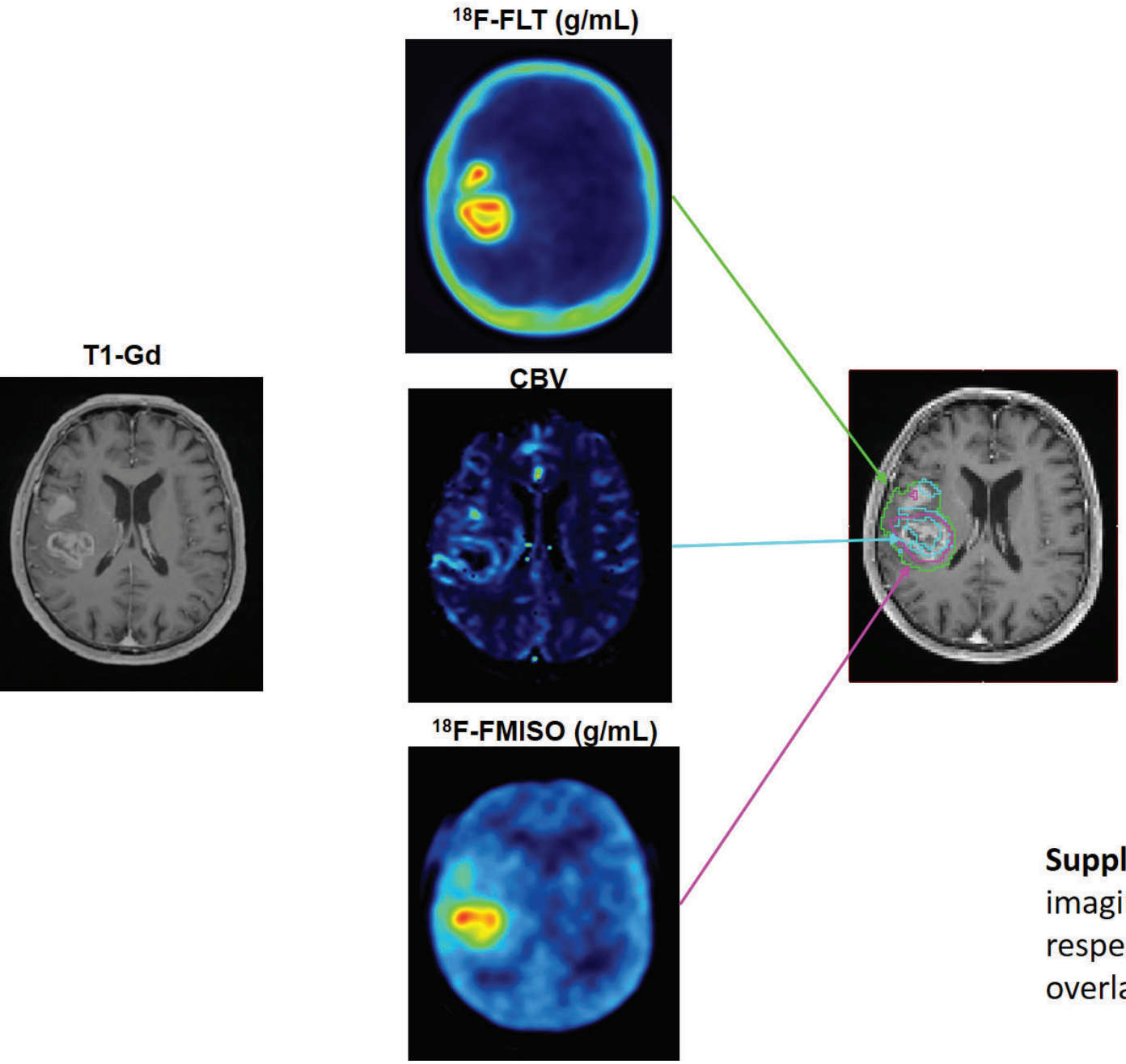

Supplemental Figure 4 : Multimodal imaging of a glioblastoma patient and the respective segmentation registered and overlayed on the T1w-Gd image.